Modelling the prestress transfer in pre-tensioned concrete elements

CrossMark

A.O. Abdelatif*, J.S. Owen, M.F.M. Hussein [1]

Faculty of Engineering, University of Nottingham, University Park, Nottingham NG7 2RD, UK

ABSTRACT

Three models were developed to simulate the transfer of prestress force from steel to concrete in pre-tensioned concrete elements. The first is an analytical model based on the thick-walled cylinder theory and considers linear material properties for both steel and concrete. The second is an axi-symmetric finite element (FE) model with linear material properties; it is used to verify the analytical model. The third model is a three dimensional nonlinear FE model. This model considers the post-cracking behaviour of concrete as well as concrete shrinkage and the time of prestress releasing. A new expression from the analytical model is developed to estimate the transmission length as well as the stress distribution along the tendon. The paper also presents a parametric study to illustrate the impact of diameter of prestressing steel, concrete cover, concrete strength, initial prestress, section size, surface roughness of prestressing steel, time of prestress release, and the member length on the transfer of stress in pre-tensioned concrete elements.

1. Introduction

The prestress force in pre-tensioned concrete elements is transferred from the steel to the concrete over a certain length, which is known as the transmission length. The formulae of the transmission length in the current design code are basically developed empirically for normal types of concrete. Because of the rapid innovation in construction industry and introducing of new types of concrete materials (i.e. high-strength, self-compacting etc.), experimental tests are needed to estimate the transmission length [1]. Models account for the new type of concrete material, based on the mechanical properties of materials which can be measured using simple tests, will be desirable [2].

The transmission length is influenced by many factors such as diameter of prestressing steel, initial or effective prestress, concrete strength, type of release, type of tendon, bond condition, concrete cover, surface condition and size of the section on the transmission length [3–11]. To date, no full agreement exists on the factors used in formulae to predict the transmission length [3].

The aim of this study is to develop a model that accounts for different concrete materials and reinforcing steel as a closed-form expression to predict the transmission length to be used in initial design stage where new concretes are used. Moreover, this study

will develop a finite element model to understand the influence of different parameters on the prestress transfer.

This paper is organised in nine sections. Sections 2 and 3 give a brief background about the previous modelling work and the transfer of prestress, respectively. In Section 4, an analytical expression to calculate the transmission length and the stress distribution is given. Axi-symmetric and 3D finite element (FE) models are developed in Sections 5 and 6. Section 7 presents a parametric study while Section 8 examines the assumptions used in the analytical model. Finally, a summary and conclusions are given in Section 9.

2. Background

Modelling the transfer of prestress force in pre-tensioned concrete elements has been described either by using empirical or numerical models (i.e. analytical and finite element (FE) models). These models allow for calculating the transmission length that is needed to transfer the prestress force in steel to concrete.

2.1. Analytical modelling background

Analytical modelling of prestress transfer was previously carried out by considering the prestressing steel as a solid cylinder and concrete as a hollow cylinder with inner radius equal to the prestressing steel radius and with an infinite outer radius [12]. Although the model assumed an infinite radius for concrete and

* Corresponding author. Currently at the University of Khartoum, Sudan.
  E-mail addresses: Amged.Abdelatif@uofk.edu (A.O. Abdelatif),
john.owen@nottingham.ac.uk (J.S. Owen), mhussein@qu.edu.qa (M.F.M. Hussein).
  [1] Currently at the University of Qatar, Qatar.

Nomenclature

A_c	cross sectional area of concrete
A_p	cross sectional area of prestressing steel
a	internal radius of cylinder
b	external radius of cylinder
d	the nominal diameter of the prestressing
dx	length of small element in longitudinal direction
E	Young's modulus
E_c	concrete Young's modulus
E_p	prestressing steel Young's modulus
e	eccentricity, which defines the rate at which the function approaches the asymptote
f_{cx}	average longitudinal stress in concrete at x
f_{cu}	concrete compressive strength after 28 days in MPa
f_{px}	longitudinal stress in prestressing steel at x
f_{bx}	bond stress at x
f_{pe}	effective prestress (beyond transmission zone)
f_{pi}	initial prestress
f_t	tensile strength
G	Drucker–Prager hyperbolic function of flow potential
G_f	fracture energy
K_c	ratio of the second invariant on the tensile meridian to that on compressive meridian
l_t	transmission length
n_p	number of mesh segments around the tendon
p	radial pressure
p_i	applied internal pressure in the radial direction
p_e	applied external pressure in the radial direction
$\bar{p}$	hydrostatic pressure
$\bar{q}$	von Mises equivalent stress
r	deformed nominal radius of the prestressing strands or bars
r_p	nominal radius of prestressing steel bar
$r_{c,1}$	internal radius of concrete cylinder which equals radius of steel bar after prestressing
$r_{c,2}$	external radius of concrete cylinder
t	age in days
T	degree of temperature
u_r	radial deformation at a radius equal r
u_r^p	radial deformation of pre-stressing bar at the outer perimeter
u_r^c	radial deformation of concrete cylinder at the inner perimeter
x	position along the transmission length
α_T	coefficient of thermal expansion
ΔT	change in temperature
ε_{sh}	shrinkage strain
ν	Poisson's ratio
ν_c	Poisson's ratio of concrete
ν_s	Poisson's ratio of steel
σ_{b0}	initial equibiaxial compressive yield stress
σ_{c0}	uni-axial compressive yield stress
$\hat{\bar{\sigma}}_{max}$	maximum principal effective stress
σ_{t0}	uni-axial tensile stress at failure
σ_z	applied stress in the longitudinal direction
τ	tangential stress
μ	coefficient of friction
ψ	angle of dilation

neglected the effect of longitudinal stress on concrete, a simple expression for prestress transfer and transmission length was given. The thick-wall cylinder model was also used to evaluate the effects of concrete cover on bond behaviour of prestressing strands in both high and normal concrete strengths considering the non-linear behaviour of concrete in tension [8]. The same concept was used to estimate the transmission length in pre-tensioned concrete element [9]. The model by Oh et al. [9] considered non-linear anisotropic concrete behaviour after the occurrence of cracks and assumed no slip. The slip of prestressing steel was considered in evaluation of the transmission length in the study of Benítez and Gálvez [1].

The literature shows that the use of the thick-wall cylinder concept in modelling of prestress transfer is simple and provides a more rational basis. On the other hand, the reviewed literature did not present a closed-form mathematical expression to estimate the transmission length and stress distribution along prestressing steel.

2.2. Finite element modelling background

The analytical modelling becomes very complicated when the material's non-linearity and the effect of different types of stresses in addition to the behaviour in 3D are taken into account. The FE method on the other hand is much more effective in handling the complexities associated with material non-linearity and the structural behaviour in 3D.

The FE method has been used by other researchers to study the effects of the releasing techniques of prestressing steel on the stress field and cracks at the end zone [13]. Kannel et al. [13] used the ABAQUS 5.4 software to model pre-tensioned concrete girders using three dimensional continuum elements for concrete and truss elements for the strands. The transfer of the prestress force from steel to concrete was modelled by varying the strand diameter linearly from zero at the end of the girder to the nominal diameter at the end of the transmission length. Another method was also used by Kannel et al. [13] in which the interactions between the steel strand and concrete were modelled by using connected rigid springs with plastic behaviour. The use of truss elements, which account only for axial forces, neglects the effect of radial deformation due to Poisson's effect. These techniques and the assumption of a linear material model for both steel and concrete do not accurately reflect the reality of the bond behaviour between prestressing steel and concrete in prestressed concrete elements.

The ANSYS FE package was also used to model pre-tensioned concrete beams and railway sleepers [14,15]. The concrete was modelled using 8-node solid elements and truss elements were used to model the prestressing steel. Concrete cracking and crushing were modelled using the concrete damage plasticity model proposed by Willam and Warnke [16]. The prestress was simulated by assigning initial strain for the truss elements while the interaction between steel and concrete surface was assumed to be fully bonded. The assumption of full bond condition affects the estimation of transfer of prestress force to concrete because it eliminates the contribution of prestressing steel slippage.

In the work of Ayoub and Filippou [17], the prestressing process was modelled across the different stages in the pre-tensioned concrete elements (i.e. prestressing, casting and releasing) using FE models in which an empirical local bond relationship was used. The main shortcoming of this model and the models before is the neglecting of the concrete tension softening behaviour.

Recently two FE approaches were developed to model the pre-tensioned concrete element, namely: the embedment approach

and the extrusion approach [18]. Both approaches implement friction-based contact surface algorithms to model the interface between steel and concrete. The approaches were modelled using the ABAQUS v.6.9 package. In the first approach, the strand was modelled as a truss element that was embedded in the concrete "embedment approach". Although this technique is less complex and has less computational cost it assumes a perfect bond and thereby neglects the possibility of strand slip. In the extrusion approach, prestressing steel was modelled using 8-node solid elements. Bond behaviour between steel and concrete was modelled using surface to surface contact element. The ABAQUS concrete damage plasticity model, which accounts for concrete post-cracking behaviour, was used to model the concrete material. The prestressing stage was effectively modelled by applying initial strain then the releasing stage was simulated by applying a strain-compatibility condition. Arab et al. [18] introduced a frictionless casting bed in their modelling to account for the effect of the self-weight in prestress transfer, although in practice, the prestressing beds always have friction. While the value of the coefficient of friction between steel strands and concrete in such models has been assumed to be 0.4 [8,9,12], Arab et al. used values of 0.7 and 1.4 based on AASHTO LRFD shear friction design recommendations.

In this paper, realistic models that consider the effects of different parameters on the transmission length are proposed. These models include a linear analytical model, which has been verified by means of an axi-symmetric FE model; both analytical and axi-symmetric models approximate the concrete around the pre-tensioned steel to a hollow concrete cylinder with thickness equal to the smallest concrete cover. This is followed by a 3D FE model which considers non-linear material models as well as the rectangular beam shape.

3. Transfer of prestress

In pre-tensioned concrete elements, when the prestress is released after hardening of concrete, the prestress force transfers gradually into the concrete. The prestressing steel tries to shorten and expands due to Poisson's ratio effect. This results in varying diameter within the transmission length in the shape of a wedge (Fig. 1).

The increment in the bar diameter imposes a normal pressure acting on the surrounding concrete. The pressure starts from high value at the end and continues decreasing along the transmission zone and reaches plateau after that (Fig. 2a). This pressure induces a frictional resistance, which acts against the shortening of the pre-tensioning steel and holds the bar/strand in tension (Fig. 2b). The forming of wedging and frictional forces is known as the *Hoyer effect* [19]. This phenomenon enhances bonding of the released prestressing steel with the surrounding concrete. As a result, the stress in steel increases gradually until it becomes constant beyond the transmission length (Fig. 2c). The distribution of compressive stress in concrete follows a similar pattern to the stress in steel (Fig. 2d), with an additional shear lag effect.
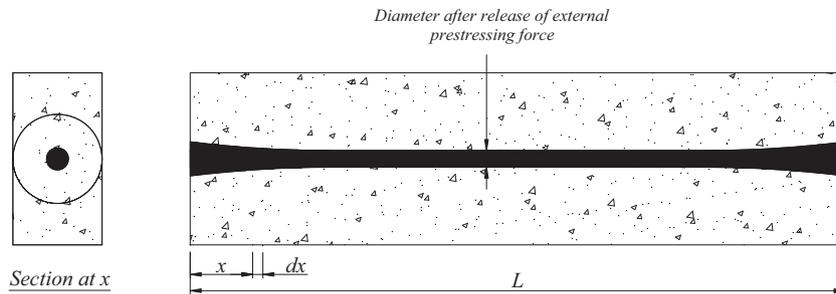

Fig. 1. Wedge action at the end of pre-tensioned concrete element.
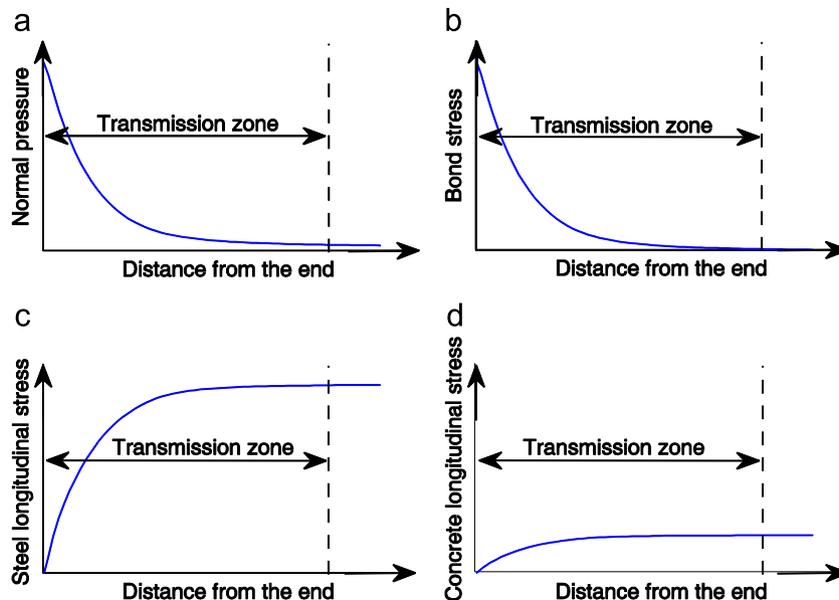

Fig. 2. Schematic stress distributions along the transmission zone: (a) normal pressure; (b) bond stress; (c) longitudinal stress in steel; and (d) longitudinal compression stress in concrete.

4. Analytical modelling

The analytical model proposed here adopts the thick-wall cylinder theory and assumes elastic material behaviour for steel and concrete [12]. The inner diameter of the concrete cylinder equals the diameter of the prestressing steel before releasing, and the outer diameter measures to the nearest concrete surface as shown in Fig. 3. The prestressing steel is modelled as a solid cylinder with a radius that equals the nominal radius of prestressing steel (strand, bar, and wire).

The thick-wall cylinder assumes that the stress is highest around the prestressing steel while the far parts have nearly zero stress. In other words; the stress contours takes a circular shape

Fig. 3. Idealisation of the thick-wall cylinder concept.

around the bar with nearly zero contours at the cylinder perimeter. This assumption will be examined in Section 8.

The prestress transfer in pre-tensioned concrete was model by examining the equilibrium, the compatibility and the bond conditions at each section. The bond between steel and concrete is modelled using Coulomb friction law. Successive solutions of these conditions along the length of the member give the distribution of prestress and the transmission length.

The flowchart in Fig. 4 shows the solution procedure for the prestress transfer model.

4.1. Equilibrium equation

To find out the distribution of stresses in a prestressing bar along the transmission length, consider a small element dx subjected to radial pressure p, axial stress f_p and bond stress as shown in Fig. 5.

From equilibrium of the force on the element:

$$\frac{df_{px}}{dx}r = 2f_{bx}. \tag{1}$$

4.2. Bond equation

Bond between steel and grout is attributed to three factors: (1) cohesion between steel and grout; (2) friction between steel and grout; and (3) mechanical resistance. The cohesion always has an insignificant influence on the load-deformation response of the structure, because the cohesion fails after a very small relative slip
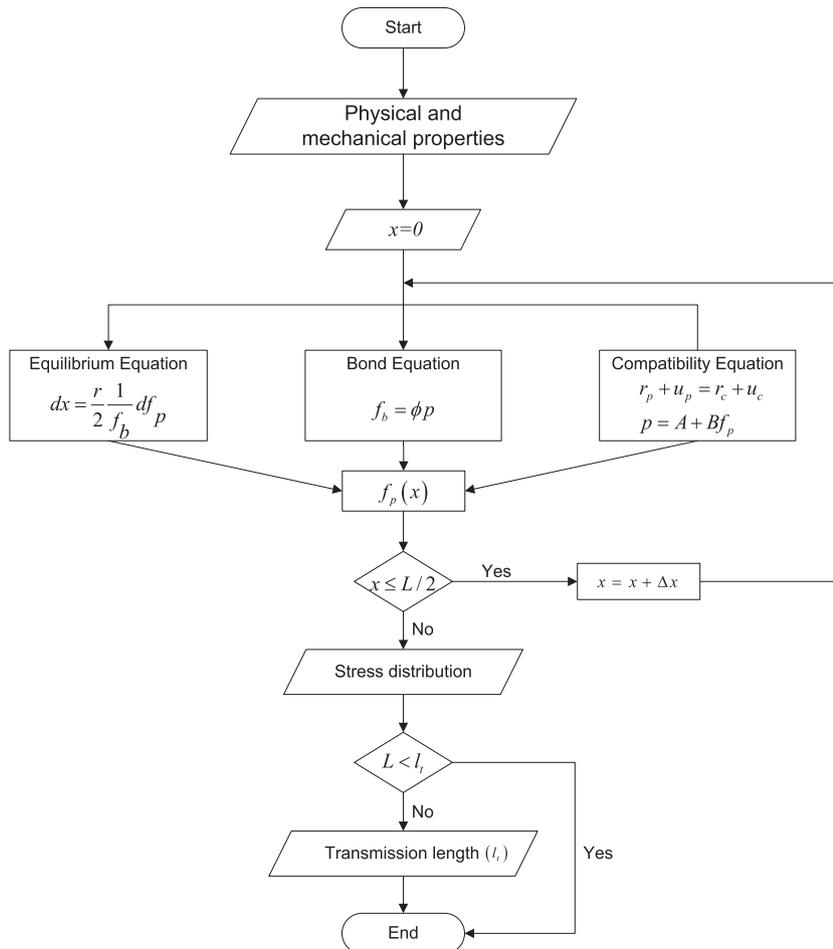

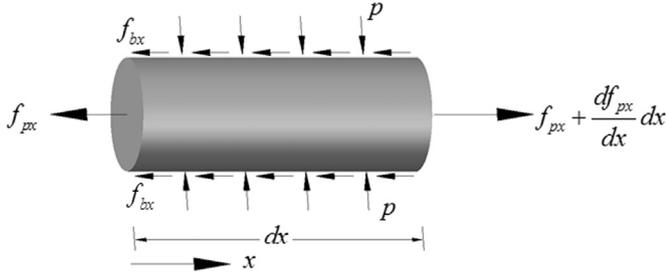**Fig. 4.** Solution procedure of the analytical model.

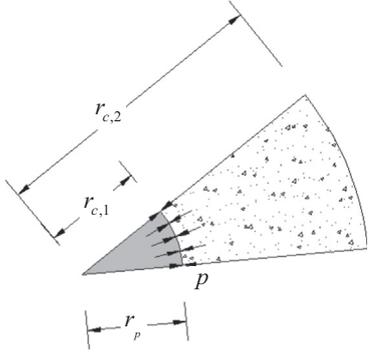Fig. 5. Stress on the pre-tensioning steel bar.

Fig. 6. Interface between concrete and pre-stressing bar.

[20,21]. The mechanical resistance only contributes to bond when deformed steel bars are used. Since a strand slips through the grout follows the pre-shaped groves without shearing off the concrete [22]. Some researchers pointed out that the contribution of the torsional stresses and lack-of-fit, from the variation in the pitch of outer strand wires, to the frictional stress is very low [22]. An empirical law was proposed by considering the so-called *pitch effect* to simulate different bond situations although the physical meaning of pitch effect is not explained [22].

Therefore, the friction between steel and grout is largely responsible for the transfer of stress into the surrounding material. According to Coulmb's friction law, bond stress can be related to the radial stress using the coefficient of friction between concrete and the steel bar as follows [8,22]:

$$f_{bx} = \mu p \tag{2}$$

The magnitude of the normal pressure p can be estimated by applying the compatibility condition at the interface between the bar and concrete.

4.3. Compatibility equation

The compatibility condition at the interfaces between the steel and concrete must be satisfied. The radial deformation of the steel at the outer radius has to equal the radial deformation of the concrete at the interior radius (Eq. (3) and Fig. 6).

$$r_p + u_r^p = r_c + u_r^c \tag{3}$$

The radial deformation of a hollow cylinder subjected to the internal, external and longitudinal stresses, as shown in Fig. 7, can be expressed as follows [23]:

$$u_r = \left[\frac{1-\mu}{E} \frac{a^2 p_i - b^2 p_e}{(b^2-a^2)} - \frac{\mu \sigma_z}{E} \right] r + \left[\frac{1+\mu}{E} \frac{a^2 b^2 (p_i - p_e)}{(b^2-a^2)} \right] \frac{1}{r} \tag{4}$$

The radial deformation of the pre-stressing steel bar can be given as follows:

$$u_{r,p} = u_r | p_i = 0; \ p_e = p; \ \sigma_z = f_{px}; \ a = 0; \ b = r_p; \ r = r_p; \ E = E_p; \ \nu = \nu_p$$

$$u_{r,p} = \frac{-p(1-\nu_p)}{E_p} r_p - \frac{\nu_p f_{px}}{E_p} r_p \tag{5}$$

For the hollow concrete cylinder, the radial deformation in the inner diameter is

$$u_{r,c} = u_r | p_i = p; \ p_e = 0; \ \sigma_z = -f_c; \ a = r_{c,1}; \ b = r_{c,2}; \ r = r_{c,1}; \\ E = E_c; \ \nu = \nu_c$$

$$u_{r,c} = \frac{p}{E_c} \frac{r_{c,1}^2}{r_{c,1}} \left[\nu_c + \frac{(r_{c,2}^2 + r_{c,1}^2)}{(r_{c,2}^2 - r_{c,1}^2)} \right] + \frac{\nu_c f_c}{E_c} r_{c,1} \tag{6}$$

Combining Eqs. (3), (5) and (6) to isolate p yields

$$p = \frac{(r_p - r_{c,1}) - \left((\nu_p f_p / E_p) r_{px} + (\nu_c f_c / E_c) r_{c,1} \right)}{((1-\nu_p)/E_p) r_p + (r_{c,1}/E_c) \left[\nu_c + ((r_{c,2}^2 + r_{c,1}^2)/(r_{c,2}^2 - r_{c,1}^2)) \right]} \tag{7}$$

The equilibrium of forces in the longitudinal direction gives

$$f_{cx} A_c = f_{px} A_p \to f_{cx} = f_{px} \frac{A_p}{A_c}$$

$$\therefore p = \frac{(r_p - r_{c,1}) - \left((\nu_p / E_p) r_p + (\nu_c / E_c) r_{c,1} (A_p / A_c) \right) f_{px}}{((1-\nu_p)/E_p) r_p + (r_{c,1}/E_c) \left[\nu_c + ((r_{c,2}^2 + r_{c,1}^2)/(r_{c,2}^2 - r_{c,1}^2)) \right]} \tag{8}$$

This equation can be rewritten in the following form:

$$p = A + B.f_{px} \tag{9}$$

where

$$A = \frac{(r_p - r_{c,1})}{((1-\nu_p)/E_p) r_p + (r_{c,1}/E_c) \left[\nu_c + ((r_{c,2}^2 + r_{c,1}^2)/(r_{c,2}^2 - _{c,1}^2)) \right]}$$

$$B = \frac{- \left((\nu_p / E_p) r_p + (\nu_c / E_c) r_{c,1} (A_p / A_c) \right)}{((1-\nu_p)/E_p) r_p + (r_{c,1}/E_c) \left[\nu_c + ((r_{c,2}^2 + r_{c,1}^2)/(r_{c,2}^2 - r_{c,1}^2)) \right]}.$$

4.4. Model solution

To solve the model, the three equations: equilibrium, compatibility, and bond, have to be solved. Substitution of the bond equation, Eq. (2) into the equilibrium equation, Eq. (1), gives

$$dx = \frac{r}{2\mu p} df_{px} \tag{10}$$

Taking into account the deformed radius of the steel bar equals

$$r = r_p + u_{r,p} = r_p + \frac{-p(1-\nu_p)}{E_p} r_p - \frac{\nu_p f_{px}}{E_p} r_p \tag{11}$$

Then, the substitution of Eqs. (9) and (11) into (10) gives

$$dx = \frac{r_p}{2\mu} \left(\frac{1}{(A+B.f_{px})} - \frac{(1-\nu_p)}{E_p} - \frac{\nu_p f_{px}}{E_p} \frac{1}{(A+B.f_{px})} \right) df_{px}.$$

The integration of the two sides of this equation yields

$$\int_0^x dx = \int_0^{f_p} \frac{r_p}{2\mu} \left(\frac{1}{(A+B.f_{px})} - \frac{(1-\nu_p)}{E_p} - \frac{\nu_p f_{px}}{E_p} \frac{1}{(A+B.f_{px})} \right) df_{px}.$$

This gives

$$x = \frac{r_p}{2\mu} \left[\frac{1}{B} \ln\left(\frac{A+B.f_{px}}{A} \right) - \left(\frac{1-\nu_p}{E_p} + \frac{\nu_p}{BE_p} \right) f_{px} - \frac{\nu_p}{B^2 E_p} \ln\left(\frac{A+B.f_{px}}{A} \right) \right]$$

$$\therefore x = \frac{r_p}{2\mu} \left[\left(\frac{1}{B} + \frac{\nu_p}{B^2 E_p} \right) \ln\left(1 + \frac{B}{A} f_{px} \right) - \left(\frac{1-\nu_p}{E_p} + \frac{\nu_p}{BE_p} \right) f_{px} \right] \tag{12}$$

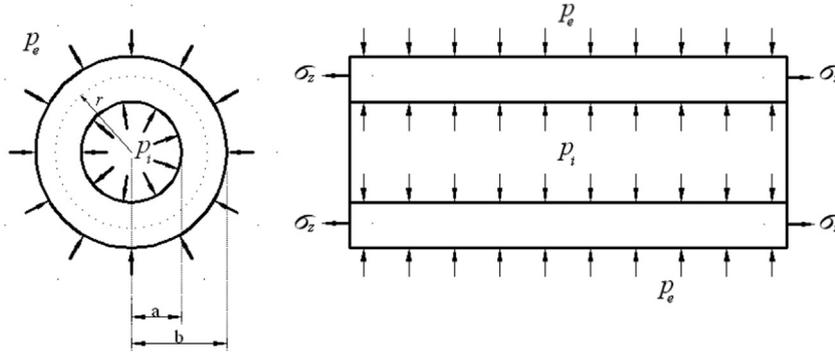Eq. (12) gives the distribution of the stress in the prestressing steel along the transmission zone.

Fig. 7. Applied pressures in a hollow cylinder.

Table 1
The parameters of the pre-tensioned concrete beam under consideration.

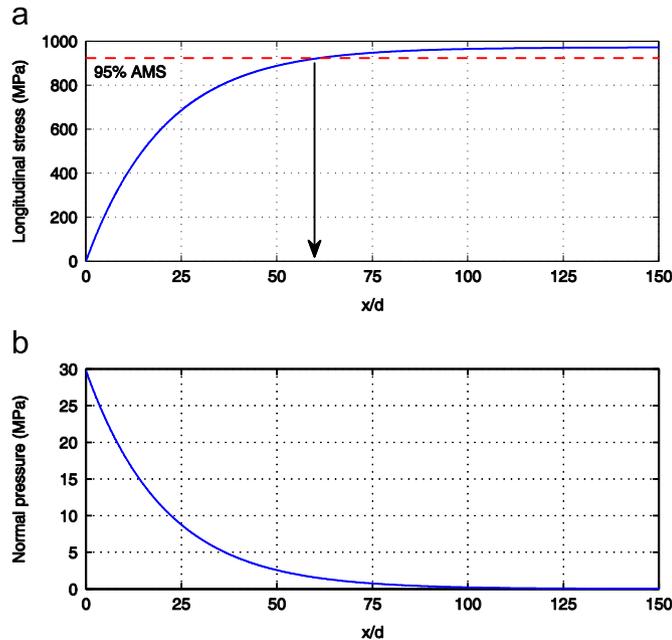| Parameter	Length (mm)	Concrete cover (mm)	Diameter of prestressing wire (mm)	Initial prestress (MPa)	Young's modulus of concrete (GPa)	Young's modulus of steel (GPa)
	3000	30	12.7	1000	30	200

Fig. 8. Longitudinal stress and the radial pressure in steel along the transmission length: (a) longitudinal stress and (b) normal pressure in steel-to-concrete interface.

The transmission length can be estimated at the intersection of a horizontal line at 95% of the average maximum strain and the strain profile at concrete surface. This method is known as 95% average maximum strain (95% AMS) method [5]. While the change in concrete strain is proportioned to the stress in the tendon after the release of external prestress force, the same concept can be applied to predict the transmission length at 95% of the maximum stress (i.e. effective stress). Therefore, the transmission length can be predicted by substitution of stress f_p in Eq. (12) with 95% of the effective prestress f_{pe}:

$$l_t = \frac{r_p}{2\mu}\left[\left(\frac{1}{B}+\frac{\nu_p}{B^2 E_s}\right)\ln\left(1+0.95 f_{pe}\frac{B}{A}\right)-0.95 f_{pe}\left(\frac{1-\nu_p}{E_p}+\frac{\nu_p}{B E_p}\right)\right] \quad (13)$$

For the pre-tensioned concrete element with the properties shown in Table 1, the steel stress profile and the normal pressure are shown in Fig. 8. Fig. 8a shows the distribution of stress in prestressing steel in the longitudinal direction. The general trend of the stress profile is exponential, which can be easily seen in Eq. (12), starting from zero at the end and yields to asymptote beyond the transmission zone. Fig. 8b illustrates the normal pressure at the interface between steel and concrete. The pressure starts from a high value at the end and decreases to nearly zero after the transmission length. This finding confirms to the concept of Hoyer's effect (i.e. wedge action).

5. FE axi-symmetric modelling of pre-tensioned concrete

A simple axi-symmetric FE model is developed using the ANSYS FE package [24]. The model's aim is to verify the proposed analytical model. Both steel and concrete were modelled as thick wall cylinders using 8-node elements with linear material properties, Fig. 9. Regarding the contact element, the contact between two bodies occurs when the normal distance between two pairs of nodes on these bodies lies within a specified tolerance. This normal distance is known as penetration, it is a direct function of the normal pressure p. When this distance is positive (i.e. gap), separation occurs and the contact pressure is set to zero. The relation between the tangential stress and the normal pressure is based on the Coulomb friction law as shown in Eq. (2). Slip on the other hand occurs when the tangential distance between the pairs exceeds the specified tolerance.

In this study the interface between steel and concrete is modelled using the surface-to-surface contact elements. Values between 0.3 and 0.7 of the coefficient of friction are reported in literature [22]. The coefficient of friction in this study was taken as 0.4 [9,12]. The allowable slip was defined when the relative displacement exceeds 1.0% of the element length across the contact surface [24].

Two solution algorithms are used to solve the contact between steel and concrete: (1) the augmented Lagrange multiplier method for solving normal contact behaviour; (2) the penalty method for solving tangential contact behaviour.

The prestressing process is modelled in three steps. In the first step, which simulates the prestressing step, an initial stress equal to the initial prestress was applied to the prestressing steel before any solution step and before concrete casting. The concrete placement is modelled by the formation of contact between steel and concrete. The third step, the prestressing steel is gradually released and a solution step takes place. A full Newton–Raphson solver with un-symmetric matrix storage was used in the static solution of the model steps.
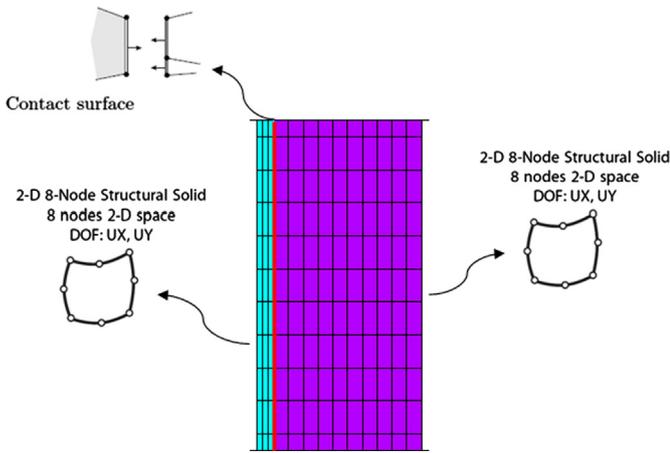
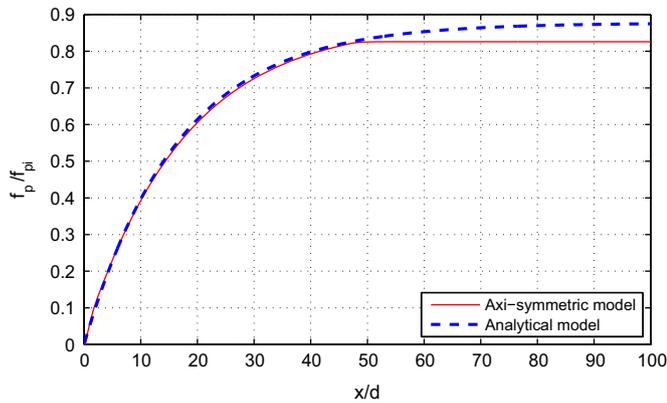**Fig. 9.** Used element and mesh on the axi-symmetric FE model.

Fig. 10. Comparison of longitudinal stress distribution between the analytical model and FE axi-symmetric model.

5.1. Verification of the analytical model

The slip of a tendon at a certain section can be defined as the relative displacement at the interface between concrete and steel cylinders. Slip of prestressing steel is likely to occur within the transmission length after the failure of cohesion between steel and concrete [25].The slip is implicitly considered in the analytical model by using of the Coulomb's friction law which is only true in the case of slippage. In order to scrutinise the impact of neglecting the compatibility in longitudinal direction, the analytical model is assessed against the axi-symmetric FE model.

As an example, consider a pre-tensioned concrete member with parameters shown in Table 1. The element size used in the mesh in this example is discretised into 200 divisions in the longitudinal direction (i.e. 15 mm), and 3 divisions (i.e. 2.12 mm) and 10 divisions (i.e. 3 mm) in radial direction in the steel and concrete, respectively. No notable improvement was observed in the results for smaller element sizes.

Fig. 10 shows a comparison between the analytical and the axi-symmetric model. Good agreement between the model solutions is observed for the transmission zone. However, there is a difference between the two models beyond the transmission zone. This is because the analytical model uses Coulomb friction law for the entire length of the member; however this is only true within transmission zone where slip/sliding of prestressing steel is present, Fig. 11a and d. The presence of slip causes a drop in the bond stress, Fig. 11b, and in the normal pressure, Fig. 11c, therefore the effective stress in the axi-symmetric FE model beyond the sliding zone, Figs. 11d and 10, is less than that in the analytical model. This finding was also observed by Den Uijl [8], who found that the slip had insignificant influence on the transmission of the prestressing force after more than 95% of the prestress is achieved. The general trend of these curves is consistent with the findings of many other researchers [8,9,12,17] and with previous experimental observations [7,9].

Fig. 11b and c also shows how the normal pressure and bond stress are proportioned according to the Coulomb's friction law.
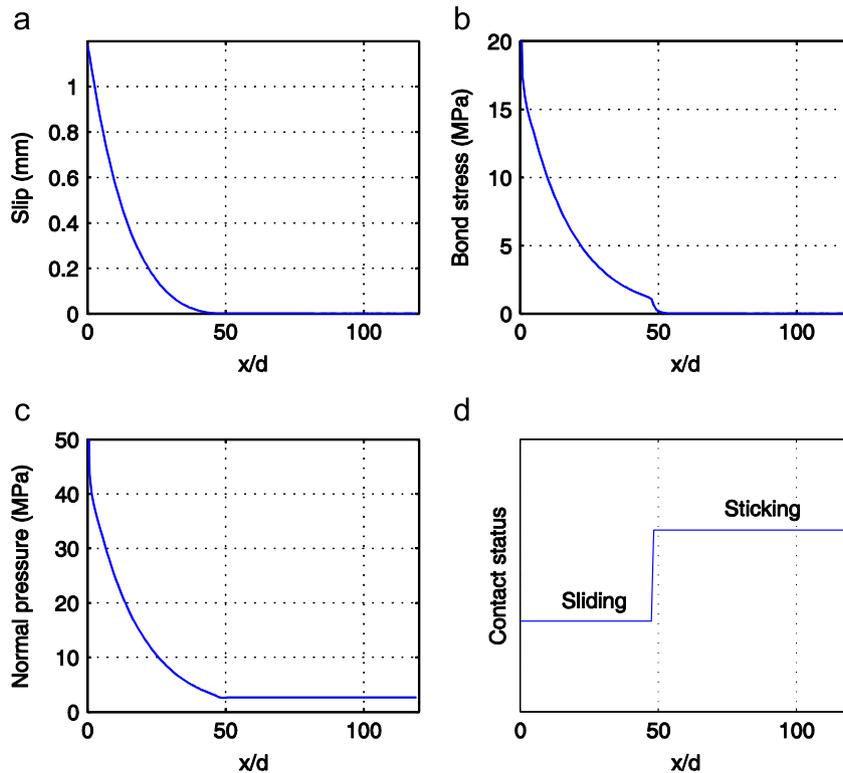

Fig. 11. Contact behaviour on the axi-symmetric FE model: (a) slip; (b) bond stress; (c) normal pressure and (d) contact status.
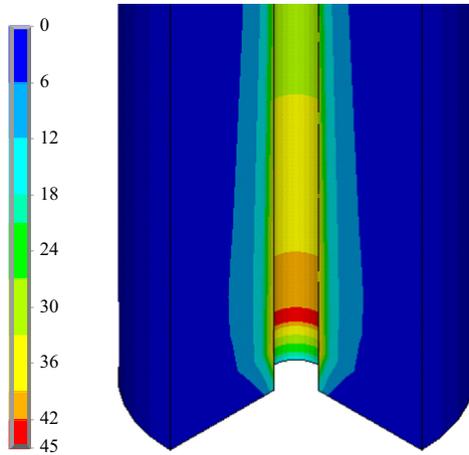
Fig. 12. Hoop stress (MPa) in concrete from axi-symmetric elastic analysis.

The presence of sliding in the entire transmission zone, Fig. 11a and d, supports the use of the static coefficient of friction.

5.2. Predicted stress in concrete

The results of the axi-symmetric FE model in Fig. 12 show that the hoop stress in the first part of the transmission length reaches values exceeding the concrete tensile strength adjacent to the tendon. This indicates that cracks will be present in the radial direction in concrete; therefore the concrete is not expected to display true elastic behaviour after cracking.

One disadvantage of the axi-symmetric modelling is that the number of radial cracks needs to be assumed (2–6 cracks) in order to account for the non-linear behaviour of concrete [26,27]. However, this phenomenon can be conveniently modelled using 3D FE analysis considering concrete non-linear behaviour.

6. 3D non-linear FE modelling of pre-tensioned concrete

A non-linear 3D model of a single-pre-tensioned concrete beam was developed using the commercial finite element package ABAQUS Version 6.10 [28]. The material models used, prestressing modelling strategy and implemented solution algorithms are discussed below.

6.1. Material models

6.1.1. Steel

Pre-tensioning steel is always stressed to a value less than the yield stress and it is, therefore, bound to behave elastically when released. Accordingly, a linear elastic material model was used for the pre-stressing steel. The pre-tensioning stress was modelled as an initial stress in the steel element as has previously been described in Section 5.

6.1.2. Concrete

The release of prestressing steel exerts radial compressive stresses and circumferential tensile stresses onto the surrounding concrete. In most practical cases, the circumferential stresses exceed the concrete tensile strength which leads to the formation of radial cracks around the prestressing steel. Therefore, the post-cracking behaviour of concrete has to be considered in the concrete material model. After prestress release, the radial stresses are always less than the compressive strength; hence, it is acceptable to use a linear model to describe the compressive behaviour of concrete.

The behaviour of concrete in tension was modelled as linear-elastic up to its tensile strength, which was taken as one-tenth of the concrete compressive strength. The post-cracking behaviour was modelled using the Hillerborg's fictitious cracking concept [29] assuming linear tension softening as shown in Fig. 13.

The fracture energy required to open a unit area of crack, G_f, was calculated as the average of the following equations [30]:

$$G_f = 43.2 + 1.13 f_{cu} \tag{14}$$

$$G_f = 30.5 + 6.64 f_t^2 \tag{15}$$

where f_{cu} and f_t are in N/mm^2 and G in N/m.

6.1.3. Concrete damage plasticity (CDP)

The concrete constitutive model used in the analysis presented in this section is the CDP model in ABAQUS (Fig. 14). The model uses the yield function proposed by Lee and Fenves [31] which is a modification of the plastic damage model of Lubliner et al. [32] to consider different strength evolution under concrete tension and compression.

6.1.4. Yield function

The yield surface function, Fig. 14, is described by the following equation [28]:

$$\frac{1}{1-\alpha}\left(\bar{q} - 3\alpha\bar{p} + \beta\left(\varepsilon^{\sim pl}\right)\langle\hat{\bar{\sigma}}_{max}\rangle - \gamma\langle-\hat{\bar{\sigma}}_{max}\rangle - \bar{\sigma}_c\left(\varepsilon_c^{\sim pl}\right)\right) = 0, \tag{16}$$

with

$$\alpha = \frac{(\sigma_{b0}/\sigma_{c0}) - 1}{2(\sigma_{b0}/\sigma_{c0}) - 1}; \quad 0 \le \alpha \le 0.5,$$

$$\beta = \frac{\bar{\sigma}_c\left(\varepsilon_c^{\sim pl}\right)}{\bar{\sigma}_t\left(\varepsilon_t^{\sim pl}\right)}(1-\alpha) - (1+\alpha),$$

$$\gamma = \frac{3(1-K_c)}{2k_c - 1}.$$

Experimental investigation shows that the ratio of σ_{b0}/σ_{c0} lies somewhere between 1.10 and 1.16 [32]. In this study the value of 1.16 was used [28]. The typical value of the K_c ratio for concrete is 2/3 [32].

6.1.5. Flow rule

The concrete stress–strain relationships and the yield surface are connected together using the flow rule. The CDP model in ABAQUS assumes non-associative potential plastic flow with
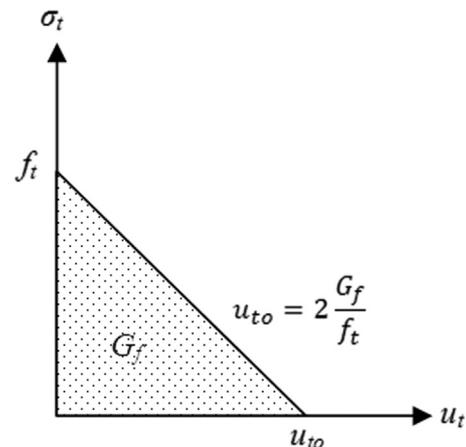

Fig. 13. Post-failure stress–fracture energy curve adopted in the 3D FE non-linear model.
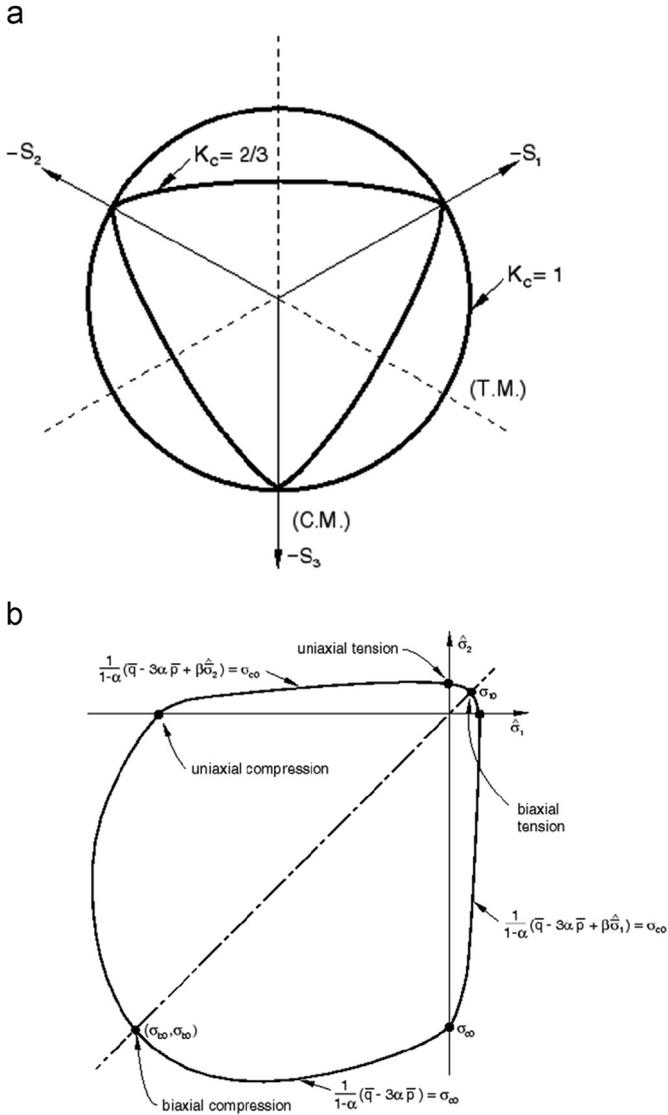
a

b

Fig. 14. Concrete damage plasticity model [28]: (a) yield surface in the deviatoric plane and (b) yield surface in plane stress.

Drucker–Prager hyperbolic function of flow potential G [28]

$$G = \sqrt{(e\sigma_{t0} \tan \psi)^2 + \overline{q}^2} - \overline{p} \tan \psi \qquad (17)$$

The eccentricity e defines the rate at which the function approaches the asymptote. A value of 0.1 eccentricity controls that the material has almost the same dilation angle ψ-measured angle in the p–q plane at high confining pressure – over a wide range of confining pressure stress values.

Lee and Fenves [31] found that when concrete was subjected to uni-axial compressive and tensile failures in both monotonic and cyclic tests, a dilation angle of 31° produces results in good agreement with the experimental ones [31]. In case of the biaxial loading tests, the angle of 31° produces a small difference in out-of-plane strain caused by larger dilatancy in comparison to the angle about 25° [31]. In the models presented here, values of 0.1 and 30° were used for the eccentricity and dilation angle, respectively.

6.1.6. Concrete shrinkage

The shrinkage of concrete is the change of volume due to loss of water. The prestress transfer on pre-tensioned concrete is known

to be affected by the concrete shrinkage. To take such effects into account the dry shrinkage strain (ε_{sh}) was estimated at a given time in days (t) using the ACI 209 R-92 model [33], Eq. (18):

$$\left. \begin{array}{l} (\varepsilon_{sh})_t = \frac{t}{t+35} \times 780 \times 10^{-6} \text{ mm/mm for moist curing} \\ (\varepsilon_{sh})_t = \frac{t}{t+55} \times 780 \times 10^{-6} \text{ mm/mm for steam curing} \end{array} \right\} \qquad (18)$$

The shrinkage of concrete was modelled as a thermal strain (ε) due to reduction in one degree of temperature (T) while the thermal coefficient of expansion (α_T) was set equal to the shrinkage strain, Eq. (19):

$$\varepsilon = \alpha_T \Delta T \qquad (19)$$

Although the relaxation of prestressing steel is not considered in this study, subtracting the relaxation losses from the initial prestress can approximate the possible behaviour.

6.2. Bond modelling and model solution

The bond between steel and concrete was modelled using surface-to-surface contact element. The Coulomb friction law was used to define the frictional behaviour between steel and concrete with a coefficient of friction of 0.4 and zero cohesion. The augmented Lagrange multiplier solver, which updates the contact stiffness any iteration, was used in solving of the contact behaviour in the normal direction of the interface while the penalty method was used to solve the contact tangential behaviour.

For solving this model under the static condition, a full Newton–Raphson solver with un-symmetric matrix storage was used. A small time step size, and therefore, a large number of increments were used to promote the convergence of the complex non-linear material behaviour and the contact problem's solution.

6.3. Mesh sensitivity

The results obtained by using the concrete damage plasticity model showed mesh dependency since the model is dependent on the concrete crack bandwidth, the width affected by the crack [28,29,31,34]. Therefore, the global response may not be identical when different element sizes are used normal to the crack direction [31]. Moreover, increasing the number of elements has been observed to result in the formation of new cracks in the localised crack zone [29]. The following strategies are recommended to reduce mesh dependency [28]:

(1) Using of fracture energy or stress displacement methods to define concrete post-cracking rather than using the stress–strain relationship. This is because the latter introduces unreasonable mesh dependency into the results in the regions lacking reinforcement.
(2) Defining the characteristic crack length to be equal to the length of a line across an element in the first order element.
(3) Use of elements with aspect ratios close to one.

In addition to the above, in this study, the effective stress was used to assess mesh sensitivity. This is because the transmission length is calculated using the 95% AMS method, which means it is not a direct result from the model.

The sensitivity of the numerical solution to the mesh discretisation was investigated in order to identify a suitable mesh. The number of segments around the steel (Fig. 15) is defined as n_p and was varied from 8 to 64. For the beam in Table 1, it was found that the effective stress values start to form a plateau for n_p greater than 40, Fig. 16. The estimated transmission length at n_p equals 40 is just 1.8% below the one for n_p equals 64. Therefore the use of n_p equals 40 gives an acceptable prediction of transmission length at
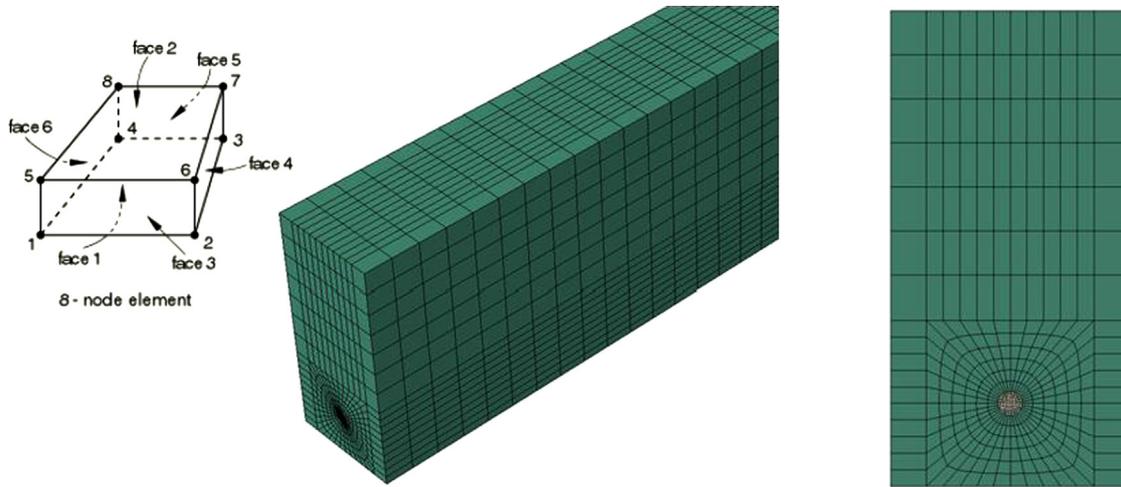
Fig. 15. Mesh density in the 3D FE model showing the element type and elements size at circumferential and in the longitudinal direction.
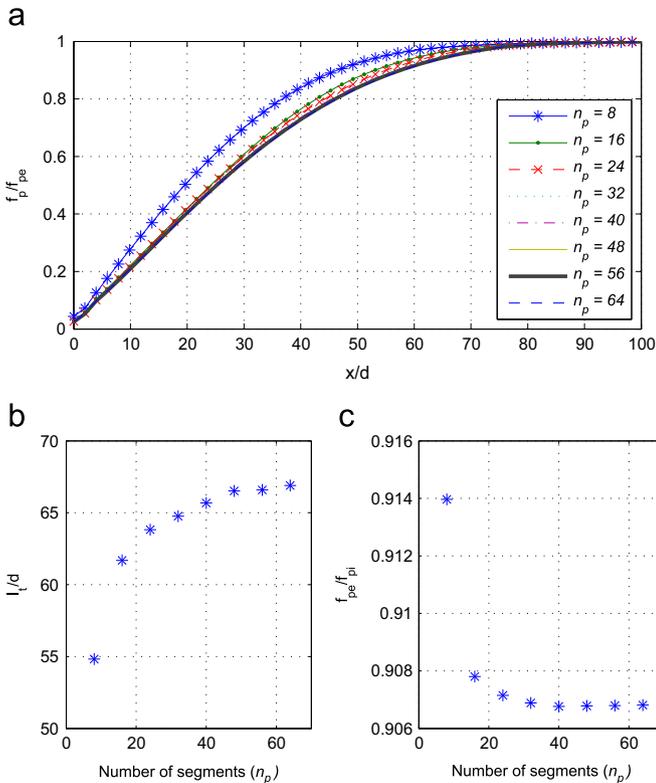

Fig. 16. Effect of the number of circumferential segments on (a) stress distribution, (b) transmission length, and (c) effective prestress.

Fig. 17. Different steps during the prestress procedure in pretensioned concrete.

6.4.1. Simulation of prestressing steps

The prestressing procedure includes three different steps. The first step is prestressing where steel is tensioned (Fig. 17a). In this step, the distribution of stresses along its length remains constant and equals the prestress magnitude (Fig. 17 – curve a). The second step is casting of concrete (Fig. 17b). After the setting of concrete, concrete shrinkage takes place causing a change to the stress profile in the pre-tensioned concrete member (Fig. 17 – curve b). In the third step the prestressing steel released (Fig. 17c). The release of the prestressing force creates radial stress and activates a frictional resistance component which enhances the transfer of prestress force into the concrete (Fig. 17 – curve c).

The influence of concrete shrinkage before releasing the prestress force is highest at the end of the element and decreases towards the centre of the element until it stabilizes to a value less than the initial prestress after a certain distance (Fig. 17 – curves a and b). This behaviour enhances the transfer of prestress although it reduces the effective prestress (Fig. 17 – curves c and d). Therefore, neglecting the effect of concrete shrinkage does not reflect the true behaviour of pre-tensioned concrete in the analysis of the prestress transfer. Furthermore, the subtraction of shrinkage losses from the initial stress in the modelling of prestress transfer does not properly account for the variation of shrinkage strain

reasonable computational cost. The sensitivity from element sizes of 25 mm, 20 mm, and 10 mm at the outer edges was also examined; no remarkable change on the model results was observed. Hence, to reduce the computational cost, the element size of 25 mm at the edges was used in this study.

6.4. Discussion of results of the 3D FE model

In this section the simulation of prestressing steps in pre-tensioned concrete elements is illustrated and the influence of concrete shrinkage on prestress transfer is shown, based on the 3D FE non-linear model. This is followed by the validations of the 3D FE model against previous experiments.
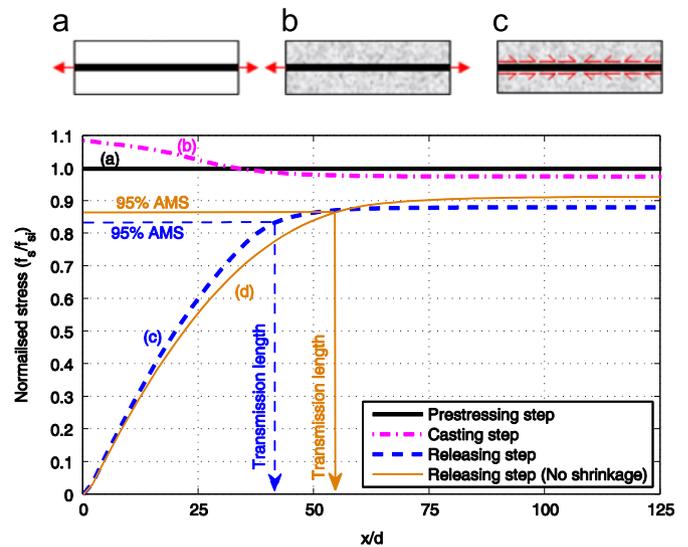
profile along the transmission length. As shown in Fig. 17, the calculation of transmission length was found to be 55.1*d* compared to 41.3*d* when concrete shrinkage before release is considered (i.e. about 25% reduction).

6.4.2. Concrete cracking along the transmission length

The release of prestressing steel usually causes radial cracks in concrete around the tendon [35]. These bursting cracks occurs due to expansion of the tendon and the wedge action [36]. In this section, the model is examined whether it is able to predict this phenomenon or not. Fig. 18 shows the visualisation of concrete cracks around the tendon and along the transmission length. The cracks are visualised here plotting the maximum principal plastic strain. It is assumed that the direction of the maximum principal plastic strain is parallel to the direction of the vector normal to the crack plane [28]. The presence of concrete cracks agrees to observations in the previous experiments [36].

6.5. Models validation

To validate the proposed models, data were compared to previous experimental results [7,9]. The comparisons exhibit a good agreement between the model and experimental measurements. As an example, Figs. 19 and 20 show comparisons of strain data normalised by the average maximum strain. In Fig. 20, the decrease of the slope of tendon stress (i.e. bond stress) can be related to the non-linear behaviour of concrete (i.e. bursting cracks), which is not considered in the analytical simulation. It can be clearly seen that the variability in measurement of experimental data and the number of measuring points between the two figures.

Mitchell et al. [7] estimated the transmission length using the slope-intercept method. The method estimates the transmission length from the end of the element to the intersection of the fitted line within the curved part of the strain profile with the horizontal fitted line of the asymptote. This method is highly dependent on how these parts are determined and the number of points in each part. For this reason only the results from 3D FE model are
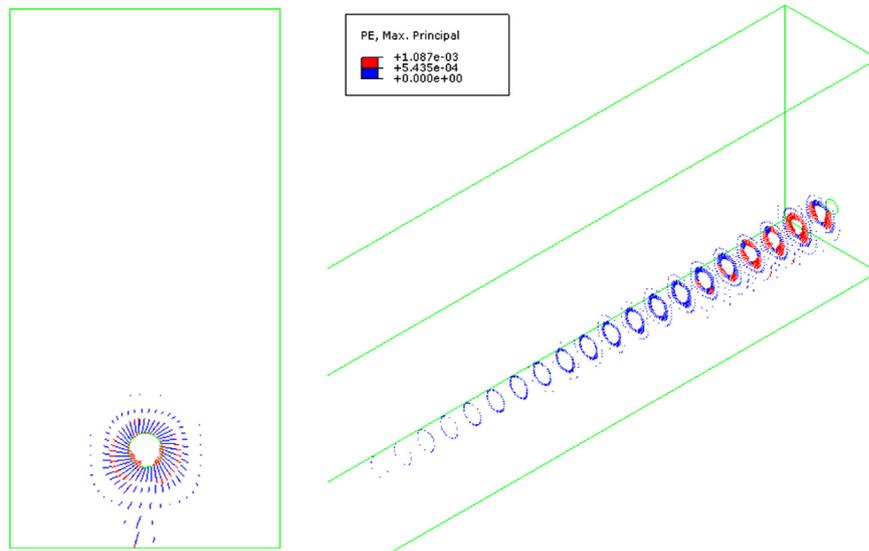

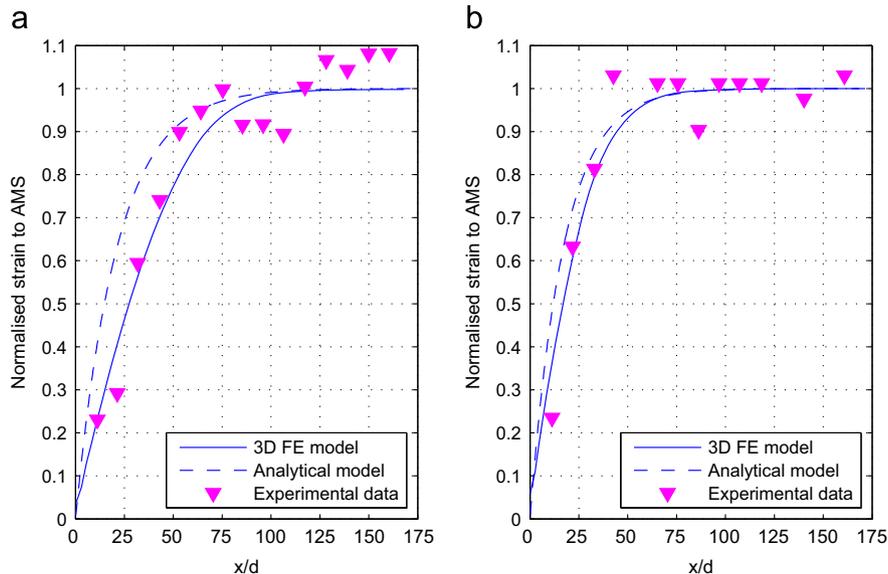**Fig. 18.** Bursting concrete crack round prestressing steel in a pretensioned concrete beam.

Fig. 19. Comparison of the models against Mitchell et al. [7] experimental data: (a) Specimen 9.5/31-1200 and (b) Specimen 9.5/89-825.
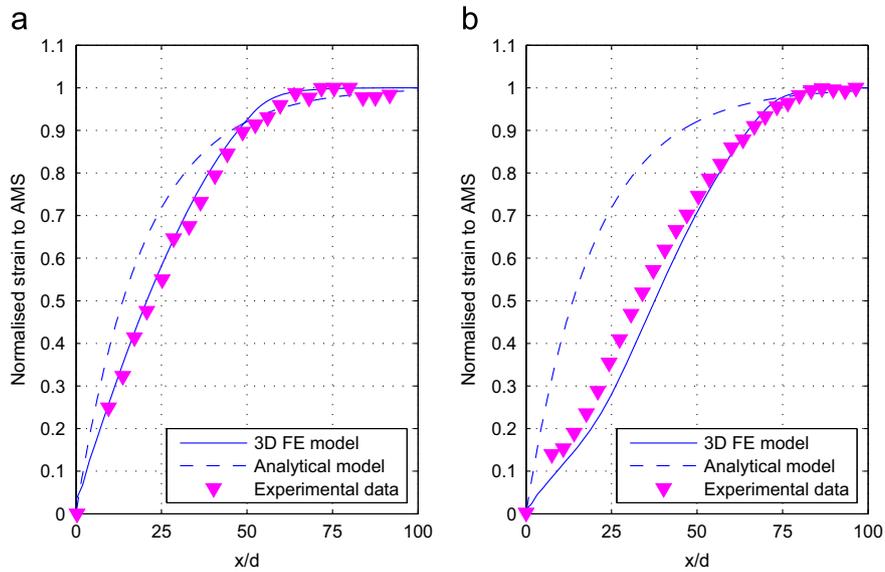
Fig. 20. Comparison of the models against Oh et al. [9] experimental data: (a) Specimen M12-N-C3-2 and (b) Specimen M15-N-C3-1.
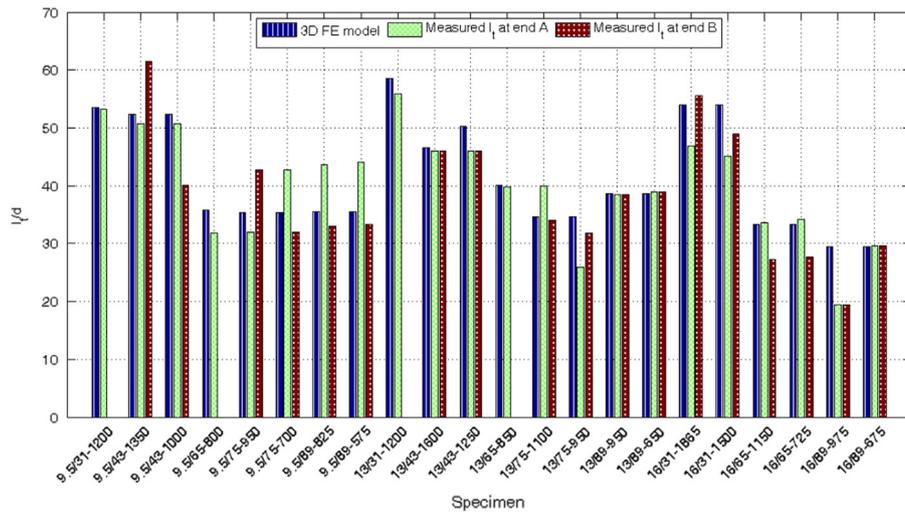

Fig. 21. Comparison of the models against Mitchell et al. [7] transmission length at the ends of beams.
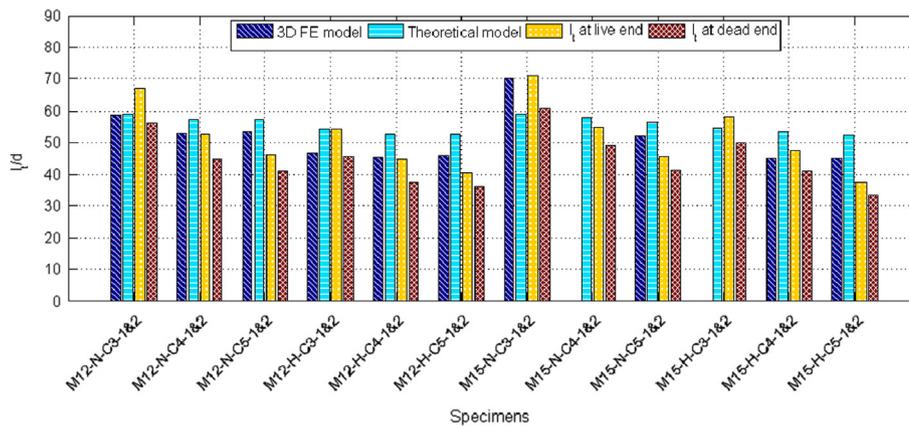

Fig. 22. Comparison of the models against Oh et al. [9] transmission length.

compared. The same method was followed to estimate the corresponding transmission length of their specimens from the FE model. Validation of the 3D FE model is carried out against 22

tests. In their published work, the transmission length was measured at the ends of each beam, i.e. end A and B, which gives 44 measurements of the transmission length (Fig. 21).

In the work of Oh et al. [9] the transmission length was estimated by predicting the transmission length at 95% of the average maximum strain (95% AMS), [5]. The comparison between the FE prediction, analytical model (i.e. Eq. (12)) and the experimental estimations of transmission length are shown in Fig. 22. Oh et al. [9] gives an estimation of each beam at the end of releasing (live end) and the far end (dead end).The comparisons against 12 specimens (i.e 24 measurements) show a reasonable agreement.

It was found that the average error on the 3D FE model predictions is less than 8% in 48 specimens. In the other hand the analytical model overestimate the transmission length by 11% based on ten specimens. However, the 3D FE model completed in about 3 h in one CPU compared to 5 ms. Take into account, in both experiments sets, the average difference in measuring the transmission length in the two ends is about 14%. Additionally, this scatter can be due to the different in the quality of the interface between steel and concrete which is influenced by many parameters such as compaction, presence of air bubbles, and mortar sedimentation. Previous reports showed 20% coefficient of variance (COV) between upper and lower bound of the transmission length in observations under similar circumstances [22]. This means that the ratio between characteristic upper and lower limit is 2.0, which indicated a high scatter in transmission length measurements in practice.

7. Parametric study

A lot of experimental work has been done to investigate the effect of different parameters on the transmission length. These investigations were carried out on a large number of beams and took a considerable amount of time. By considering the cost of experimental parametric studies as well, it is more convenient to assess the influence of different parameters on the transmission length using numerical models. In the following sections the influence on the transmission length due to the change in prestressing steel diameter, concrete strength, initial prestress, concrete cover, cross-section size, time of prestress release, surface roughness, and the member length are shown. Comparison is also made between the findings of the current study and previous observations. The properties of beams used are shown in Table 2. In this study it is assumed that all beams are subjected to moist curing. The Young's modulus of steel is taken as 200 GPa while the concrete Young's modulus is estimated using [37]

$$E_c = 20 + 0.2 \times f_{cu}. \tag{20}$$

The Poisson ratio for steel and concrete is taken as 0.3 and 0.2, respectively.

The study focuses on the influences on the transmission length and on the effective prestress (i.e. maximum stress along the tendon after release) as well. The transmission length is normalised to the diameter of the pre-tensioning steel (d) while the effective prestress (f_{pe}) is normalised to the initial prestress (f_{pi}).

The parametric study is performed on a high performance computing cluster using eight CPUs with 16 GB of RAM. This has reduced the computational time drastically and has allowed for a number of parameter to be studied.

7.1. Diameter

The results of the model show that in case of constant concrete cover, the transmission length increases proportionally with an increase of diameter (Fig. 23). The same conclusion was made by other researchers [5,38]. This observation can be also demonstrated by Eq. (13). On the other hand the effective prestress slightly decreases with increase of the tendon diameter within a range less than 6% of the initial prestress.

7.2. Concrete strength

Fig. 24 shows the influence of concrete compressive strength at release on prestress transfer in pre-tensioned concrete. It is found that the increase of concrete compressive strength reduces the transmission length and increases the effective prestress. This is because of increasing concrete tensile strength and Young's modulus as a result of increasing the compressive strength. The increase of tensile strength reduces the cracked concrete zone around prestressing steel and thereby enhances the transfer of the prestress force. A similar observation was also reported by Mitchell et al. [7] who investigated experimentally the influence of high concrete strength on the transmission length. The increase of compressive strength from 25 MPa to 50 MPa results only in about 3% increase in the effective prestress.
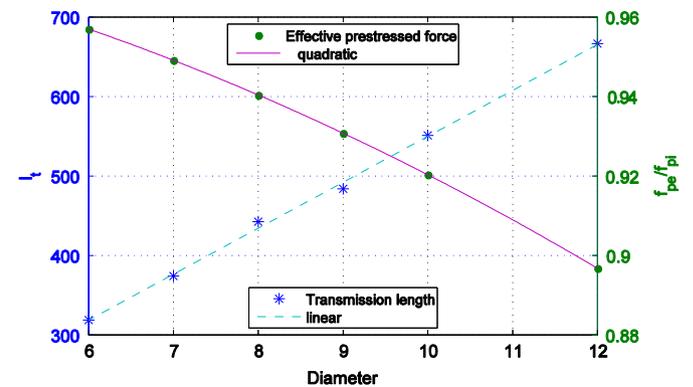

Fig. 23. Influence of prestressing steel diameter with constant cover on the transmission length.

Table 2
The considered beam properties to study each parameter.

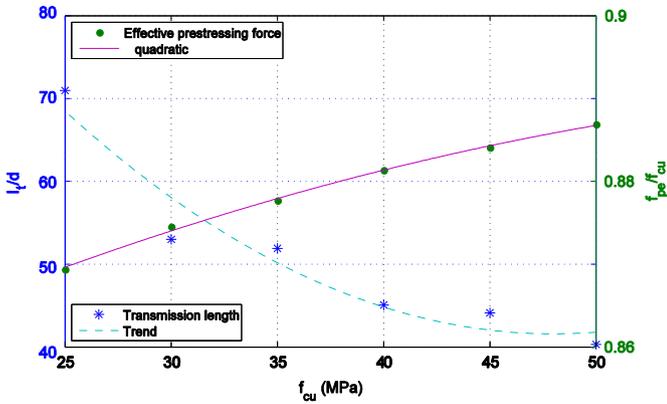| Parameter	b (mm)	h (mm)	L (mm)	Diameter (mm)	Cover (mm)	Compressive strength (MPa)	Initial prestress (mm)
Diameter	100	200	1600	Varies	30	40	1400
Concrete strength	100	200	1600	12.7	30	Varies	1000
Initial prestress	100	200	1600	12.7	30	40	Varies
Concrete cover	200	200	1600	10	Varies	40	1400
Cross-section	100	Varies	1600	10	30	40	1400
Time of release	100	200	1600	12.7	30	40	1400
Surface roughness	100	200	1600	12.7	30	40	1250
Length	100	200	Varies	12.7	30	40	1400

Fig. 24. Influence of concrete strength on the transmission length.
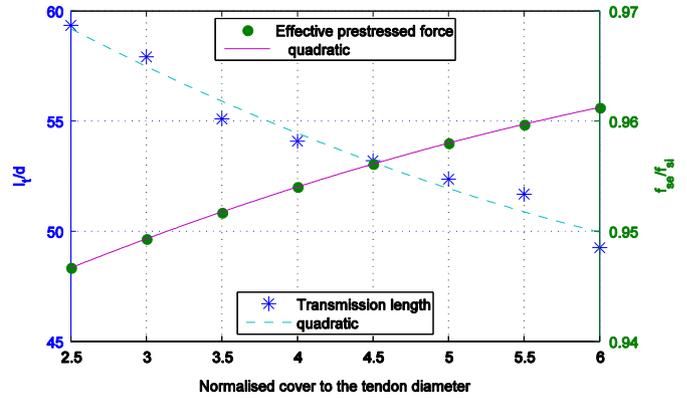

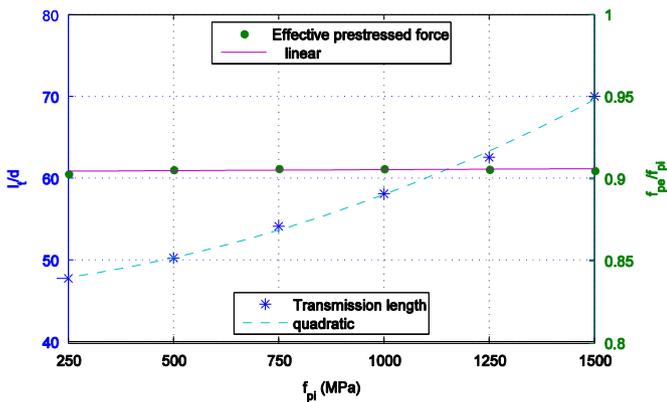**Fig. 26.** Influence of cover on the transmission length.

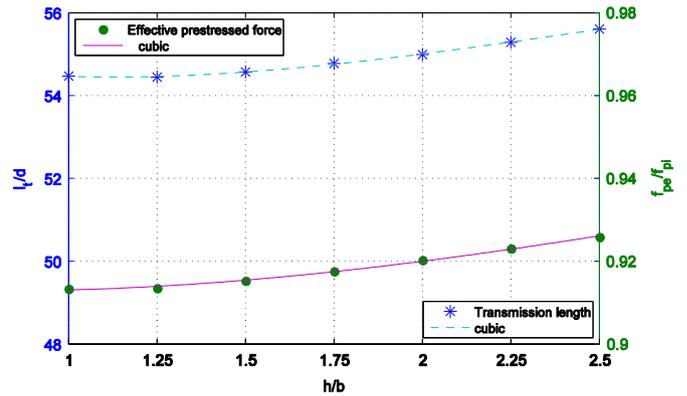**Fig. 25.** Influence of initial prestress on the transmission length.

Fig. 27. Influence of the size of cross-sectional area on the transmission length.

7.3. Initial prestress

The radial expansion of prestressing steel due to Poisson's effect after the release of prestressing force is in direct proportion with the magnitude of the initial prestress. The increasing of the initial prestress force causes an increase in the magnitude of circumferential stresses around the prestressing steel and hence the concrete cracking. As a result, the length that is required to transfer the prestress force becomes longer as is demonstrated in Fig. 25. This observation is supported by Eq. (13). It can also be seen that in all beams the effective prestress force develop to the same percentage.

7.4. Concrete cover

Fig. 26 shows a possible trend of influence of concrete cover on the transmission length. The final point (i.e. at 6d) was excluded from the curve fit as it appears to be an outlier. A Similar trend was observed in previous experiments conducted by Oh and Kim [6]. It is found that the transmission length decreases with the increase of the concrete cover (Fig. 26). This is caused by the increase of nonlinearity in concrete and decrease of frictional resistance at the interface in the case of small covers [8]. Only less than 2% change was observed in the effective prestress in this case. The trend also shows that the reduction in the transmission length reached a plateau beyond a concrete cover of 5.5d in this simulation. However, Den Uijl has reported no further reduction to be expected beyond 3d to 4d [8].

7.5. Cross-sectional area of concrete

Russell and Burns [5] reported that large elements with multiple strands have a shorter transmission length. However,
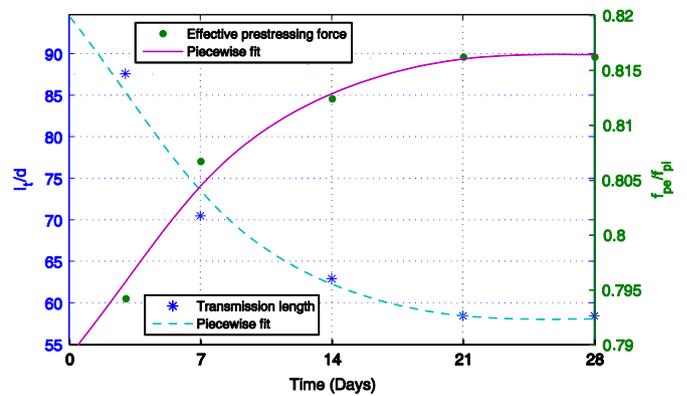

Fig. 28. Influence of releasing time on the transmission length.

for a pre-tensioned beam with a single strand, the results show that the size of the section does not affect either the transmission length or the effective prestress significantly (Fig. 27). This contradiction can be attributed to the fact that their experimental observations were based on a comparison between various beams with different number of strands, and different concrete properties and shapes (i.e. rectangular and I-beams). Also, this can be related to the presence of the transverse reinforcement which enhances the concrete confinement and bond behaviour.

7.6. Time of release

Ageing of the concrete causes an increase in the concrete compressive strength, tensile strength, Young's modulus and

shrinkage strain, which results in enhanced bond between steel and concrete. In this investigation, it was found that later release of external prestress force results in shorter transmission length and up to 3% higher effective prestress, Fig. 28. No considerable change in either transmission length or effective prestress was observed after 21 days.
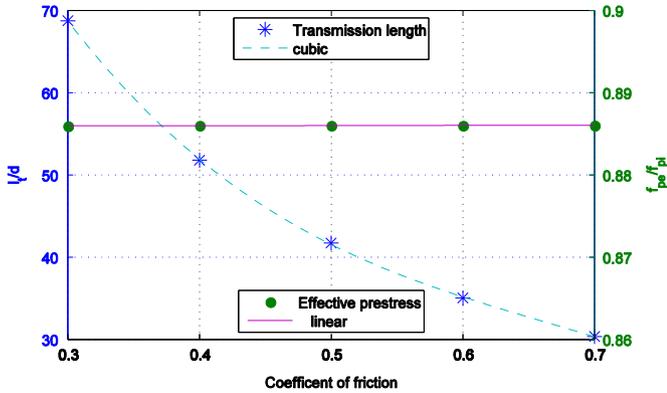

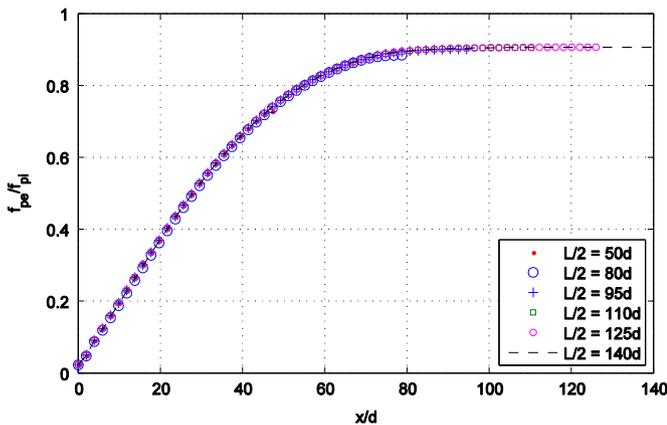**Fig. 29.** Influence of the tendon surface roughness on the prestress transfer.

Fig. 30. Influence of the length of the member on the transmission length.

7.7. Surface roughness of prestressing steel

It is well known that the increase of steel roughness due to the presence of rust on the steel enhances the bond between steel and concrete [39]. To investigate the influence of surface roughness the coefficient of friction in the model is varied between 0.3 and 0.7 [22]. Fig. 29 shows that pre-tensioned concrete elements with a rough surface tendon have a smaller transmission length in comparison to those with a smooth surface. This finding was also reported in Ref. [40]. In the figure, it also can be observed that the tendons in all cases develop to the same stress level, which means the surface roughness has no influence on the effective prestress.

7.8. Length of pre-tensioned member

In case half of the length of a member is less than the transfer length, it is found that the stress distribution follows the full transmission curve up to the stress corresponding to the half-length, Fig. 30. This finding is very helpful when experiments are designed, especially if the aim of the test is studying the bond behaviour in the end zone rather than focusing on measuring of the transmission length. Note that although there is no slip at the member's half-length, the change in steel strain is not equal to the concrete strain.

8. Assessment of using the thick-wall cylinder concept in modelling prestress transfer

The developed 3D FE model was also used to examine the thick-wall cylinder assumption for prestressed concrete. A contour plot of von Mises stresses shows the concentration of stress around the prestressing steel. The von Mises contours take a circular shape and they diminish at a distance approximately equal to the concrete cover, Fig. 31. This observation means the assumption that the prestressing steel is a solid cylinder surrounded by a hollow thick-wall cylinder is acceptable.

More investigations are carried out on beams with different cross section and constant concrete cover of 30 mm (i.e. 3d) as shown in Fig. 32. The beams with a width of 100 mm and depth vary from 125 mm up to 250 mm (Table 2). Fig. 32 shows similar
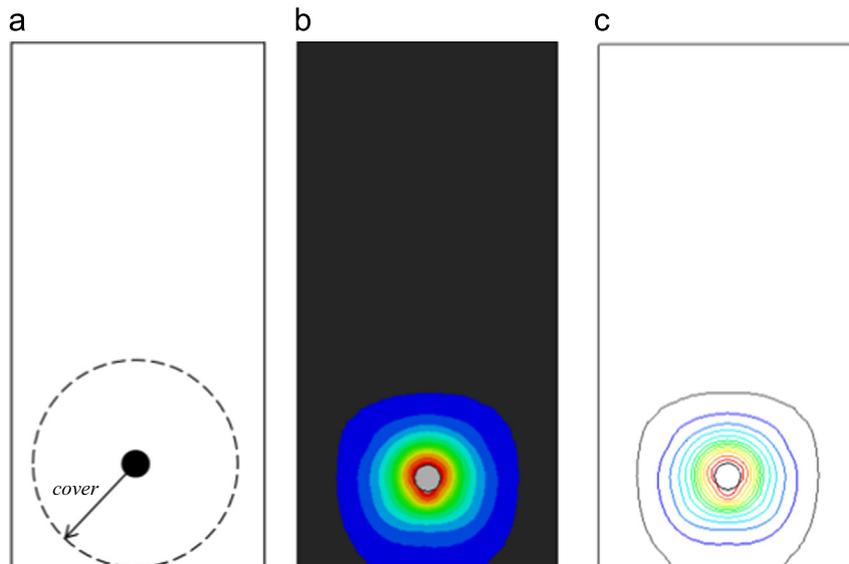

Fig. 31. (a) Assumption of thick-wall cylinder, (b) and (c) von Mises stress contour at the end of pre-tensioned concrete element.
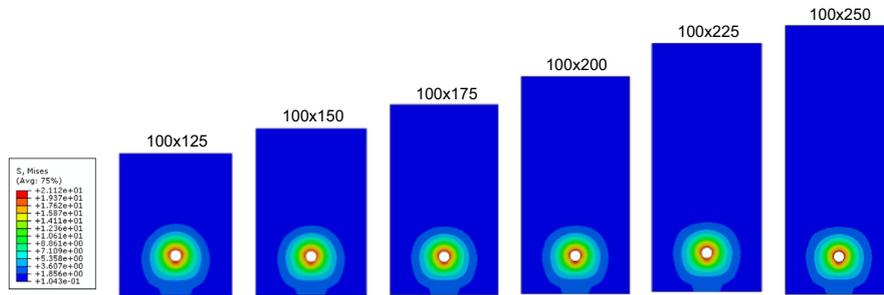
Fig. 32. von Mises stress contours in beams with constant concrete cover (3d) and different cross section.
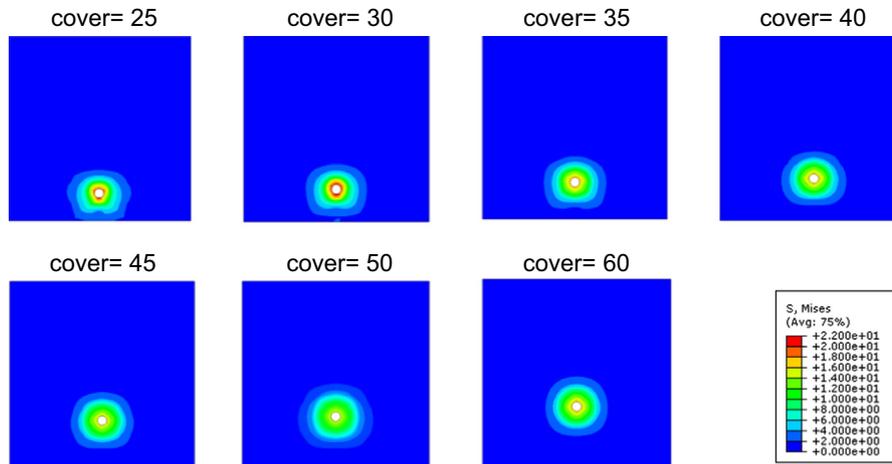

Fig. 33. Variation of von Mises stress contours with concrete cover (10 mm tendon diameter).

stress contours for all beams. This result is also supporting the findings in Section 7.5, which shows that the prestress transfer is not dependant on the size of the pre-tensioned concrete unit in the case of equal covers.

Also the von Mises contours are plotted for the 200×200 mm^2 beams with different concrete cover shown in Section 7.4 (Fig. 33). In this case, also circular contours are observed around the tendon with different intensity. The beams with smaller concrete cover show higher level of stress compare to those with the larger cover.

9. Conclusions

A closed-form expression of the transmission length is presented in this paper based on a linear analytical model and the thick-wall cylinder theory. The paper also presents a 3D non-linear FE model considering the post-cracking behaviour of concrete in addition to different parameters such as concrete cover, initial prestress, concrete strength, concrete shrinkage and member cross section. It is found that the 3D non-linear finite element model is more accurate than the analytical model although the analytical model is more computationally efficient.

The developed 3D FE model was then used to examine the assumptions of the thick-wall cylinder model to simulate the prestress transfer in pre-tensioned concrete elements which was found to be reliable. This model is also used to investigate the influence of prestressing steel diameter, concrete cover, concrete strength, initial prestress, section size, member length, time of prestress releasing, and surface condition of the tendon on the transfer of prestress force from steel to concrete in pre-tensioned concrete elements.

The following conclusions can be drawn:

- A linear closed-form expression has been proposed to predict the transmission length and the stress profile along the transmission zone. The proposed expression can be used in the initial design stage where new concrete materials are used and there is an absence of code-design formulae. The 3D non-linear FE model can be used as a tool to understand the phenomenon of prestress transfer considering different aspects.
- In the modelling of prestress transfer, it is not appropriate to account for the concrete shrinkage by subtracting the shrinkage losses from the initial prestress. Concrete shrinkage before release imposed non-uniform increase (at the end) and decrease (far from the end) of stresses along the member. The use of the thick-wall cylinder theory was found to be reliable in modelling the prestress transfer.
- The presented parametric study, based on the 3D FE model, provides useful information about the influence of steel diameter, concrete cover, concrete strength, initial prestress, section size, member length, time of prestress releasing, and surface condition of the tendon on the transfer of prestress force from steel to concrete in pre-tensioned concrete elements.
- The size of the element was found to have no significant effect on the prestress transfer

In general, the paper has drawn advanced numerical simulations to improve the understanding of the prestressed transfer in pre-tensioned concrete. It has also proposed an analytical formula

of the transmission length as well the stress distribution over the transmission zone.

Acknowledgement

References

[1] J. Benítez, J. Gálvez, Bond modelling of prestressed concrete during the prestressing force release, Mater. Struct. 44 (2011) 263–278.

[2] P.G. Gambarova, Bond in reinforced concrete: where do we stand today?, in: W. Cairns, G. Metelli, G.A. Plizzari (Eds.), Bond in Concrete 2012: Bond, Anchorage, Detailing, Brescia, Italy, 2012, pp. 1–13.

[3] J.R. Martí-Vargas, et al., Bond of 13 mm prestressing steel strands in pretensioned concrete members, Eng. Struct. 41 (0) (2012) 403–412.

[4] fib, Model Code 2010, Fédération Internationale du Béton fib/International Federation for Structural Concrete, 2010.

[5] B.W. Russell, N.H. Burns, Design guidelines for transfer, development and debonding of large diameter seven wire strands in pretensioned concrete girders, in: Research Report 1210-5F, Center for Transportation Research, the University of Texas at Austin, Austin, Texas, 1993.

[6] B.H. Oh, E.S. Kim, Realistic evaluation of transfer lengths in pretensioned prestressed concrete members, ACI Struct. J. 97 (6) (2000) 821–830.

[7] D. Mitchell, et al., Influence of high strength concrete on transfer and development length of pretensioning strand, PCI J. 38 (3) (1993) 52–66.

[8] J. Den Uijl, Bond modelling of prestressing strand, ACI Spec. Publ. 180 (1998) 145–169.

[9] B.H. Oh, E.S. Kim, Y.C. Choi, Theoretical analysis of transfer lengths in pretensioned prestressed concrete members, J. Eng. Mech. 132 (10) (2006) 1057–1066.

[10] ACI Committee 318, Building code requirements for reinforced concrete (ACI 318-08), in: American Engineering and Industrial Standards, American Standards Association, New York, NY, United States, 2008.

[11] BS EN, Eurocode 2: Design of Concrete Structures: Part 1-1: General Rules and Rules for Buildings, British Standards Institution, 2004.

[12] J.R. Janney, Nature of bond in pre-tensioned prestressed concrete, Am. Concr. Inst. J. 26 (4, Part 2) (1954) 736-1.

[13] J. Kannel, C. French, H. Stolarski, Release methodology of strands to reduce end cracking in pretensioned concrete girders, PCI J. 42 (1) (1997) 42–54.

[14] S. Kaewunruen, A. Remennikov, Nonlinear finite element modelling of railway prestressed concrete sleeper, in: Proceedings of the 10th East Asia-Pacific Conference on Structural Engineering and Construction, Bangkok, Thailand, 2006.

[15] A.J. Wolanski, Flexural Behavior of Reinforced and Prestressed Concrete Beams Using Finite Element Analysis, Faculty of the Graduate School, Marquette University, Milwaukee, United States, 2004.

[16] K. Willam, E. Warnke, Constitutive model for the triaxial behavior of concrete, in: Proceedings of the International Association for Bridge and Structural Engineering, 1975, p. 174.

[17] A. Ayoub, F.C. Filippou, Finite-element model for pretensioned prestressed concrete girders, J. Struct. Eng. 136 (2010) 401.

[18] A.A. Arab, S.S. Badie, M.T. Manzari, A methodological approach for finite element modeling of pretensioned concrete members at the release of pretensioning, Eng. Struct. 33 (6) (2011) 1918–1929.

[19] V. Briere, et al., Dilation behavior of seven-wire prestressing strand – the Hoyer effect, Constr. Build. Mater. 40 (0) (2013) 650–658.

[20] P. Marti, et al., Temporary corrosion protection and bond of prestressing steel, ACI Struct. J. – Am. Concr. Inst. 105 (1) (2008) 51–59.

[21] J. Cairns, Y. Du, D. Law, Influence of corrosion on the friction characteristics of the steel/concrete interface, Constr. Build. Mater. 21 (1) (2007) 190–197.

[22] fib, Bond of reinforcement in concrete, in: State of Art Report, International Federation For Structural Concrete, 2000.

[23] S.P. Timoshenko, in: N.Y. Huntington, E. Robert (Eds.), Strength of Materials, 3rd ed.,Krieger Pub. Co, Lausanne, Switzerland, 1976 (442 pp.).

[24] ANSYS Inc., Theory Reference for the Mechanical APDL and Mechanical Applications Release 12.0, Canonsburg, PA, 2009.

[25] J.R. Marti-Vargas, et al., Reliability of transfer length estimation from strand end slip, ACI Struct. J. 104 (4) (2007) 487–494.

[26] K. Lundgren, Bond between ribbed bars and concrete. Part 1: modified model, Mag. Concr. Res. 57 (7) (2005) 371–382.

[27] M. Ruiz, A. Muttoni, P. Gambarova, Analytical modeling of the pre- and postyield behavior of bond in reinforced concrete, J. Struct. Eng. 133 (10) (2007) 1364–1372.

[28] Dassault Systemes Simulia, ABAQUS 6.10 Documentation Collection, Dassault Systemes Simulia Corp., Providence, RI, USA, 2010.

[29] A. Hillerborg, M. Modéer, P.E. Petersson, Analysis of crack formation and crack growth in concrete by means of fracture mechanics and finite elements, Cem. Concr. Res. 6 (6) (1976) 773–781.

[30] D. Phillips, Z. Binsheng, Direct tension tests on notched and un-notched plain concrete specimens, Mag. Concr. Res. 45 (162) (1993) 25–35.

[31] J. Lee, G.L. Fenves, Plastic-damage model for cyclic loading of concrete structures, J. Eng. Mech. 124 (8) (1998) 892.

[32] J. Lubliner, et al., A plastic-damage model for concrete, Int. J. Solids Struct. 25 (3) (1989) 299–326.

[33] ACI-209, Prediction of Creep, Shrinkage and Temperature Effects in Concrete Structures, ACI 209 R-92, 1992.

[34] B. Koeberl, Question of tension softening versus tension stiffening in plain and reinforced concrete, J. Eng. Mech. 134 (9) (2008) 804.

[35] A. Nanni, M. Tanigaki, K. Hasuo, Bond anchorage of pretensioned FRP tendon at force release, J. Struct. Eng. 118 (10) (1992) 2837–2854.

[36] D.Y. Moon, et al., On strain change of prestressing strand during detensioning procedures, Eng. Struct. 32 (9) (2010) 2570–2578.

[37] J. Newman, B.S. Choo, Advanced Concrete Technology Set, Butterworth-Heinemann, Oxford, UK, 2003.

[38] P. Zia, T. Mostafa, Development length of prestressing strands, PCI J. 22 (5) (1977) 54–65.

[39] C. Fang, et al., Corrosion influence on bond in reinforced concrete, Cem. Concr. Res. 34 (11) (2004) 2159–2167.

[40] R.W. Barnes, J.W. Grove, N.H. Burns, Experimental assessment of factors affecting transfer length, ACI Struct. J. 100 (2003) 6.